Response of GPS occultation signals to atmospheric gravity waves and retrieval of gravity wave parameters

Y. A. Liou · A. G. Pavelyev · J. Wickert · C. Y. Huang · S. K. Yan · S. F. Liu

Abstract We show that the amplitude of the Global Positioning System (GPS) signals in the radio occultation (RO) experiments is an indicator of the activity of the gravity waves (GW) in the atmosphere. The amplitude of the GPS RO signals is more sensitive to the atmospheric wave structures than is the phase. Early investigations used only the phase of the GPS occultation signals for statistical investigation of the GW activity in the height interval 10–40 km on a global scale. In this study, we use the polarization equations and Hilbert transform to find the 1-D GW radio image in the atmosphere by analyzing the amplitude of the RO signal. The radio image, also called the GW portrait, consists of the phase and amplitude of the GW as functions of height. We demonstrate the potential of this method using the amplitude data from GPS/Meteorology (GPS/MET) and satellite mission Challenge Minisatellite Payload (CHAMP) RO events. The GW activity is nonuniformly distributed with the main contribution associated with the tropopause and the secondary maximums related to the GW breaking regions. Using our method we find the vertical profiles of the horizontal wind perturbations and its vertical gradient associated with the GW influence. The estimated values of the horizontal wind perturbations are in fairly good agreement with radiosonde data. The horizontal wind perturbations v(h) are ±1 to ±5 m s with vertical gradients dv/dh ±0.5 to ±15 m s km at height 10–40 km. The height dependence of the GW vertical wavelength was inferred through the differentiation of the GW phase. Analysis of this dependence using the dispersion relationship for the GW gives the estimation of the projection of the horizontal background wind velocity on the direction of the GW propagation. For the event considered, the magnitude of this projection changes between 1.5 and 10 m s at heights of 10–40 km. We conclude that the amplitude of the GPS occultation signals contain important information about the wave processes in the atmosphere on a global scale.

Keywords Radio occultation · Amplitude method · Gravity waves

Received: 6 August 2003 / Accepted: 5 March 2004
Published online: 6 May 2004

Y. A. Liou (✉) · A. G. Pavelyev · J. Wickert
C. Y. Huang · S. K. Yan · S. F. Liu
Center for Space and Remote Sensing Research,
National Central University, 320 Chung-Li, Taiwan
E-mail: yueian@csrsr.ncu.edu.tw
Tel.: +886-3-4227151
Fax: +886-3-4254908

Introduction

The gravity waves (GW) in the atmosphere have been observed and modeled for many years (Nagpal 1979). The small-scale GW with wavelengths of a few kilometers and periods near 10 min are generated in the planetary boundary layer (Nagpal 1979). The medium-scale GW with horizontal wavelengths of about 100–1,000 km, vertical wavelengths of 1–10 km, and periods of 10 min to 1 h, are mainly produced owing to the weather activities (fronts, cyclones, cumulonimbus convection, thunderstorms) and wind flows over irregular topography (mountain waves). They play a decisive role in transporting energy and momentum, in contributing turbulence and mixing, and in affecting the atmospheric circulation and temperature regimes (Fritts and Alexander 2003). The breaking and dissipation of the GW play an important role for the dynamics of the mesosphere (Ebel 1984). For a realistic description of the climate changes and variations in the atmospheric, stratospheric, and mesospheric global-scale flows, dynamical simulation studies of the stratosphere and mesosphere require a broad spectrum of knowledge including the GW effects on the empirical models or analytic formulations (Preusse et al. 1996).
Radiosonde and rocketsonde GW measurements, balloon soundings, radar observations and lidar studies have been limited to ground-based sites (Eckermann et al. 1995; Sica and Russell 1999) mainly over specific land areas of the

Northern Hemisphere. Recently, a few high-resolution stratospheric satellite instruments have been used to detect GW (Eckermann and Preusse 1999). However, the time for observations has been limited. This raises the problem of insufficient data for establishing wave climatology for a global scale, despite the good results from many of the ground-based and space-borne instruments (Steiner and Kirchengast 2000).

For the investigation of the internal wave activity in the atmosphere, radically new radio occultation technology can be used. This technology incorporates the high-precision radio signals of the GPS at two frequencies F1=1,575.42 and 1,227.6 MHz. The small satellites (e.g., MicroLab-1, installed into a near polar circular orbit with altitude of about 750 km) carried a laptop-sized GPS receiver to perform remote sensing of the atmosphere and ionosphere by the limb sounding method (Ware et al. 1996; Feng and Herman 1999). The advantages of the space-borne observations of the earth's atmosphere by the GPS radio signals propagating through the mesosphere and stratosphere, are that the RO technique can recover atmospheric profiles above oceans as well as above land with high-vertical resolution (<0.4 km) and accuracy (<1 K in temperatures within the upper troposphere and lower stratosphere; Anthes et al. 2000). Nowadays, new satellite missions CHAMP and SAC-C have been launched to elaborate the new RO method of global control on the meteorological processes in the atmosphere and phenomena in the ionosphere (Wickert et al. 2001; Reigber et al. 2002). In order to find the vertical gradients of the refractivity and temperature in the atmosphere with high accuracy and spatial resolution, which is important for the GW investigation, radio holographic technology has been proposed and validated (Pavelyev et al. 2002a, 2002b; Liou et al. 2002, 2003).

Analysis of the temperature variations found from the RO phase data furnishes an opportunity to investigate the global morphology of the GW activity in the stratosphere and to measure the GW statistical characteristics in the atmosphere as shown by Tsuda et al. 2000; Steiner and Kirchengast 2000; and Tsuda and Hocke 2002. However, these papers were concerned mainly with the GW statistical parameters. The amplitude channels of the RO signal offer new potential and capability for RO research and for the observation of the quasi-regular structures in the atmospheric and ionospheric waves (Kalashnikov et al. 1986; Pavelyev et al. 2002a, 2002b; Sokolovskiy 2000; Igarashi et al. 2000, 2001; Liou et al. 2002). Using the wave trains in the amplitude of the RO signals, Liou et al. (2003) introduced a new analytical method to express the amplitude and phase of the GW as functions of height in the troposphere and stratosphere. They connected the amplitude and phase of the wave trains in the RO amplitude data with the amplitude and phase of the GWs using the polarization and dispersion equations for the GW and the Hilbert transform. This method opens new perspectives for the GW investigation in the atmosphere and mesosphere using the RO data; and as a consequence, its capabilities and limitations should be analyzed in more detail. The aims of this paper are to describe the connections between the RO amplitude variations and the amplitude and phase of the GW, and to demonstrate the possibility of direct observation of the quasi-regular internal waves in the atmosphere using the amplitude of the RO signals.

Length of coherent interaction of RO signal with the atmosphere

The scheme of the RO experiment is shown in Fig. 1. Point O is the center of the spherical symmetry of the atmosphere. The radio waves emitted by the GPS satellite (point G) are propagating to the receiver onboard of the LEO satellite (point L) along the ray GTL, where T is the tangent point in the atmosphere. At point T, the ray's distance from the Earth's surface is minimal. The projection of point T on the Earth's surface determines the coordinates of the RO region: latitude ϕ and longitude λ. The vicinity of the point T introduces the major contribution to the changes of the RO signal. Record of the RO signal along the LEO trajectory contains the amplitudes A1(t) and A2(t) and phases of the radio field at frequencies F1 and F2 as functions of time. The time interval for the RO measurements τ depends on the orientation between the vertical direction at the point T and the occultation beam path. The time τ is minimal, about 30 s, when the orbital planes of the LEO and GPS satellites are parallel. Thus the RO experiments record the impact of the GW on the RO signal almost simultaneously because the GW frequencies are usually well below $1/\tau$, i.e., 0.03 s^{-1}. The RO method is appropriate for the observation of the GW in the atmosphere and ionosphere (Tsuda et al. 2000; Steiner and Kirchengast 2000; Tsuda and Hocke 2002; Igarashi et al. 2000, 2001; Pavelyev et al. 2002b; Liou et al. 2002, 2003). For application of the RO method to the wave analysis, it is desirable to estimate the horizontal and vertical resolution depending on the horizontal Λ_h and vertical wavelength Λ_v. The horizontal resolution of the RO method is connected with the length of the coherent interaction L_c between the RO signal and the atmosphere (Igarashi et al. 2001). In the case of spherical symmetry, the main contribution to the RO signal introduces a relatively small essential area with the center at the ray tangent point T (Fig. 1). At this point, the direction angle α of the ray

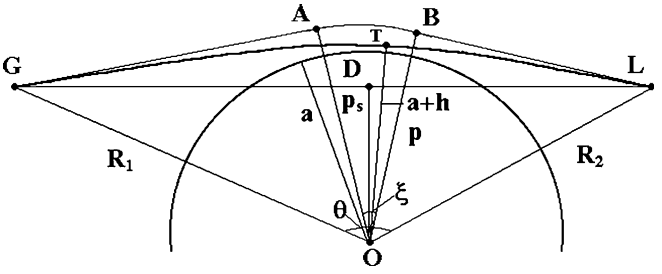

Fig. 1
Scheme of radio occultation experiment

trajectory relative to the local vertical is zero, and the radio waves propagate nearly along the layer (Igarashi et al. 2001). Because the ray inside the essential zone is nearly perpendicular to the vertical gradient of the refractivity d $N(r)$/dr one can define L_c as an effective parameter from equation $L_c = |\xi(p)n(r)/[\mathrm{d}\,N(r)/\mathrm{d}r]|$ where $\xi(p)$ is the refraction angle, p is the ray impact parameter, and $n(r)$ is the refraction index at point T (Fig. 1). Using the analytic expressions for $\xi(p)$ and $N(r)$ given in the radio-physical model (Pavelyev et al. 1996; Pavelyev 1998), one can estimate the value $L_c=(2\pi rH)^{1/2}$ for the case of the standard atmosphere with effective scale height H where r is the distance from the tangent point T to the center of spherical symmetry O (Fig. 1). For a periodical wave structure in the atmosphere, having the vertical period Λ_v, the model gives $L_c=(r\Lambda_v)^{1/2}$, and L_c is diminishing as a square root of Λ_v. One obtains for H=8 km, Λ_v=1 km, $r\approx$6370 km the values $L_c\approx$580 km and $L_c\approx$80 km respectively. Propagation of the radio waves along the essential area introduces an averaging effect within a vertical size of the Fresnel zone $\Delta h=(\lambda X L_c/4)^{1/2}=(\lambda X/4)^{1/2}(r\Lambda_v)^{1/4}$ where X is the refraction attenuation in the intensity of the radio wave. For Λ_v=1 km, λ=20 cm, and X=1 we obtain $\Delta h\approx$64 m. This value of Δh characterizes the intrinsic vertical resolution of the RO method. The intrinsic resolution Δhdepends on the vertical period of the wave structure Λ_v, and changes from 64 to 124 m when Λ_v varies in the range 1–16 km.
Note that the term "intrinsic resolution" may correspond to the experimental resolution in the case when the observations are near the essential zone. As a consequence, the intrinsic resolution corresponds to the extreme value of the vertical resolution, which can be achieved, in principle, in the RO experiments. One can estimate the lower diffractive limit of the length of the essential area L_c and the value α at its boundary. The angle α is connected with L_c by $\alpha=0.5L_c/r$. For coherent interaction of the radio wave with a layered structure at T the difference $\alpha-\xi(\alpha)=\alpha(1-\mathrm{d}\xi/\mathrm{d}\alpha)=\alpha M_d$ must not exceed the angular size of the Fresnel zone at point T (Fig. 1) where $M_d=M'_r(r)/n(r)$ and $M(r)=n(r)r$ is proportional to the modified refraction index $n(r)r/a$. From these relations one can obtain a condition $\alpha \le (\lambda X/L_c)^{1/2} M_d$. At the boundary of the concerned area both values are equal and one can find α and L_c as $\alpha=2^{-1/3}(\lambda X/r)^{1/3}M_d^{-2/3}$and $L_c=2^{2/3}r^{2/3}\lambda^{1/3}X^{1/3}M_d^{-2/3}$, and then $\Delta h=L_c[\alpha-\xi(\alpha)]/2$ or $\Delta h=2^{-2/3}r^{1/3}\lambda^{2/3}X^{2/3}M_d^{1/3}$. In the case X=1 and $M_d\approx$1 one obtains $\Delta h=2^{-2/3}r^{1/3}\lambda^{2/3}$. For X=1, λ=20 cm, $M_d\approx$1, $r\approx$6,370 km we get $L_c\approx$32 km and $\Delta h\approx$40 m. It follows from this analysis that the lower diffractive limit of the intrinsic horizontal resolution of the RO method depends on the wavelength of the radio waves λ, the radius of the curvature of the layered structure in the atmosphere r, and the vertical gradient of the modified refraction index M_d, but not dependent on the vertical wavelength of the internal wave Λ_v. When $M_d\approx$0 the length of coherent interaction can be high. This corresponds to the phenomenon of wave-guide propagation with strong diffraction effect. Under typical conditions the physical optics formulas for the intrinsic horizontal resolution $L_c=(r\Lambda_v)^{1/2}$ and vertical resolution $\Delta h=(\lambda X/2)^{1/2}(r\Lambda_v)^{1/4}$are valid. They indicate a dependence of L_c and Δhon the vertical wavelength Λ_v of the internal wave as $\Lambda_v^{1/2}$ and $\Lambda_v^{1/4}$, respectively. One can obtain an expression for the critical value of the vertical wavelength Λ_{vc}, when the coherent lengths L_c found from the physical optics and diffractive limit coincide, as $\Lambda_{vc}=2^{4/3}r^{1/3}\lambda^{2/3}X^{2/3}M_d^{2/3}\approx$160 m using $X=M_d$=1, λ=20 cm, and $r\approx$6,370 km. It is important that this analysis makes the local character of the RO method clear, and shows the upper boundaries for the physically realizable resolution in the vertical and horizontal directions, which can be achieved in the RO investigation of the internal waves in the atmosphere and ionosphere.

Sensitivity of the amplitude and phase of RO signal to wave structures

In the case of a spherical symmetric medium the RO signal propagates in the RO plane GOL, and the RO ray can be described by a plane curve GTL with a constant impact parameter p. The straight line GDL is the ray trajectory in free space with the free space impact parameter p_s (Fig. 1). To obtain the connection between the amplitude and phase variations we will compare the expressions for the phase path excess $\Phi(p)$ and the refraction attenuation X(p) for the case of one center of the spherical symmetry. The phase path excess associated with the RO ray GTL (Fig. 1) can be presented in the form:

$$\Phi(\mathrm{p}) = \mathrm{L}(\mathrm{p}) + \kappa(\mathrm{p}) + \delta(\mathrm{p}) \tag{1}$$

$$\delta(\mathrm{p}) = \mathrm{L}_1(\mathrm{p}) + \mathrm{L}_2(\mathrm{p}) - \mathrm{L}_3(\mathrm{p}) - \mathrm{L}_4(\mathrm{p}) \tag{2}$$

$$\mathrm{L}_{1,2}(\mathrm{p}) = \left[\mathrm{n}^2(\mathrm{R}_{1,2})\mathrm{R}_{1,2}^2 - \mathrm{p}^2\right]^{1/2}, \mathrm{L}_{3,4}(\mathrm{p}) = \left(\mathrm{R}_{1,2}^2 - \mathrm{p}^2\right)^{1/2} \tag{3}$$

$$\mathrm{L}(\mathrm{p}) = \mathrm{L}_1(\mathrm{p}) + \mathrm{L}_2(\mathrm{p}) - \mathrm{L}_3(\mathrm{p}) - \mathrm{L}_4(\mathrm{p}) + \mathrm{p}\xi(\mathrm{p}) \tag{4}$$

$$\xi(\mathrm{p}) = \mathrm{A}(\mathrm{p}) - \mathrm{A}(\mathrm{p_s}) \tag{5}$$

$$\mathrm{A}(\mathrm{p}) = \sin^{-1}\{\mathrm{p}/[\mathrm{n}(\mathrm{R}_1)\mathrm{R}_1]\} + \sin^{-1}\{\mathrm{p}/[\mathrm{n}(\mathrm{R}_2)\mathrm{R}_2]\} \tag{6}$$

$$\mathrm{A}(\mathrm{p_s}) = \sin^{-1}(\mathrm{p_s}/\mathrm{R}_1) + \sin^{-1}(\mathrm{p_s}/\mathrm{R}_2) \tag{7}$$

$$\kappa(\mathrm{p}) = -\int_{\mathrm{r_o}}^{\mathrm{R}_2} \mathrm{n}'_\mathrm{r}/\mathrm{n}(\mathrm{n}^2\,\mathrm{r}^2 - \mathrm{p}^2)^{1/2}\mathrm{d}\mathrm{r} - \int_{\mathrm{r_o}}^{\mathrm{R}_1} \mathrm{n}'_\mathrm{r}/\mathrm{n}(\mathrm{n}^2\,\mathrm{r}^2 - \mathrm{p}^2)^{1/2}\mathrm{d}\mathrm{r} \tag{8}$$

where r_o is the distance OT (Fig. 1) and $\delta(p)$ is the local refractivity part of the phase path excess depending on the plasma density at points G and L. If the refraction indexes $n(R_2)$ and $n(R_1)$ at the point G and L are equal to unity then $\delta(p)$=0. $L(p)$ in Eq. (4) is the geometrical part of the phase path excess equal to the difference between the geometrical lengths of the curve GABL and straight line

GDL (Fig. 1), and $\kappa(p)$ is the main refractivity part of the phase path excess depending only on the height distribution of the refractivity. The main refractivity part of the phase path excess $\kappa(p)$ is connected with the bending angle $\xi(p)$ by a relationship

$$-\mathrm{d}\kappa(\mathrm{p})/\mathrm{dp} = \xi(\mathrm{p}) \tag{9}$$

For the refraction attenuation of the RO signal intensity we use the formulas obtained early by Pavelyev and Kucherjavenkov (1978),

$$\mathrm{X(p)} = \mathrm{pR_0^2[R_1R_2L_1(p)L_2(p)\sin\theta]^{-1}}\ |\partial\theta/\partial\mathrm{p}|^{-1} \tag{10}$$

$$\theta = \pi + \xi(\mathrm{p}) - \mathrm{A(p)} \tag{11}$$

$$\partial\theta/\partial\mathrm{p} = -\mathrm{p}^{-1}\partial\Phi/\partial\mathrm{p} = \mathrm{d}\xi/\mathrm{dp} - 1/\mathrm{L_1(p)} - 1/\mathrm{L_2(p)} \tag{12}$$

where R_0 is the distance GDL (Fig. 1). Relationships Eqs. (10) and (12) connect the phase path excess and the refraction attenuation. It follows from Eqs. (10) and (12) that one can determine, in principle, the refraction attenuation from the phase path excess data because of connections Eq. (12) between the partial derivatives with respect to the impact parameter p of the phase path excess $\Phi(p)$, central angle $\theta(p)$, and refraction angle $\xi(p)$. As a consequence, Eqs. (10) and (12) indicate that the refraction attenuation and the amplitude data contain all information needed for retrieving the vertical refractivity profiles. The refraction attenuation $X(p)$ can be written in a more simple form (Pavelyev et al. 1996):

$$\begin{aligned}\mathrm{X(p)} &= \mathrm{p/p_sL_3(p_s)L_4(p_s)/[L_2(p)L_1(p)]}\ |\partial\theta/\partial\mathrm{p_s}|/|\partial\theta/\partial\mathrm{p}| \\ &\approx |\partial\theta/\partial\mathrm{p_s}|/|\partial\theta/\partial\mathrm{p}|\end{aligned} \tag{13}$$

$$\partial\theta/\partial\mathrm{p_s} = -1/\mathrm{L_3(p_s)} - 1/\mathrm{L_4(p_s)} \tag{14}$$

The refraction attenuation $X(p)$ in Eq. (13) depends mainly on the derivative of the refraction angle $\mathrm{d}\xi(p)/\mathrm{d}p$ because the changes in the impact parameters p and p_s are relatively small, about ±2% in the RO experiments. As a consequence, the refraction attenuation $X(p)$ practically does not depend on the geometrical part of the phase path excess $L(p)$ and on the local refractivity part $\delta(p)$. The refraction attenuation $X(p)$ depends mainly on the second derivative of the main refractivity part of the phase path excess $\kappa(p)$:

$$\begin{aligned}\mathrm{X(p)} = &\left[1/\mathrm{L_3(p_s)} + 1/\mathrm{L_4(p_s)}\right]/|\mathrm{d^2}\kappa/\mathrm{dp^2} + 1/\mathrm{L_1(p)} \\ &+ 1/\mathrm{L_2(p)}|\end{aligned} \tag{15}$$

The main refractivity part of the phase path excess $\kappa(p)$ in Eq. (8) contains all the information about the vertical refractivity distribution needed for the solution of the inverse RO problem: finding the refractivity vertical profile from the phase path excess data. The functions $L(p)$ and $\delta(p)$ can be considered as systematic errors that depend on the form of the path in the ionosphere and on the local refractivity variations near the transmitter and receiver.

The amplitude of the RO signal is free from natural systematic errors connected with functions $L(p)$ and $\delta(p)$ and depends mostly on the second derivative of the main phase path excess $\kappa(p)$. As a consequence, the amplitude of the GPS occultation signal has an advantage of being more sensitive to the wave structures in the atmosphere than are the phase data. However, the amplitude data depend on technical shortcomings such as the receiver noise, multipath antenna effect, instability in the transmitter's power, and receiver's gain. Despite these technical errors, the amplitude of the RO signal is a valuable source of information about ionospheric and atmospheric parameters (Pavelyev et al. 2002a, 2002b; Liou et al. 2002, 2003).

Response of amplitude variations to wave structures in the atmosphere

The amplitudes of the RO signal are shown in Fig. 2 for the CHAMP RO event 0005 (curve A) and GPS/MET RO event 0316 (curves A1, A2). Results of the simulations of the amplitude dependence on height are shown in Fig. 2 by the curves M0 and M. For calculating M0 we used the refractivity model $N(h)=N_o\exp(-h/H)$ with $N_o=340$ (N-units) and $H=6.4$ km, and the analytical connection between the refraction angle $\xi(p)$, the length of coherent interaction, and the refractivity gradient described above in Section 2. For calculating the refraction attenuation, we applied Eqs. (10) and (12). We applied the same method to obtain the curves M in Fig. 2, but the refractivity model

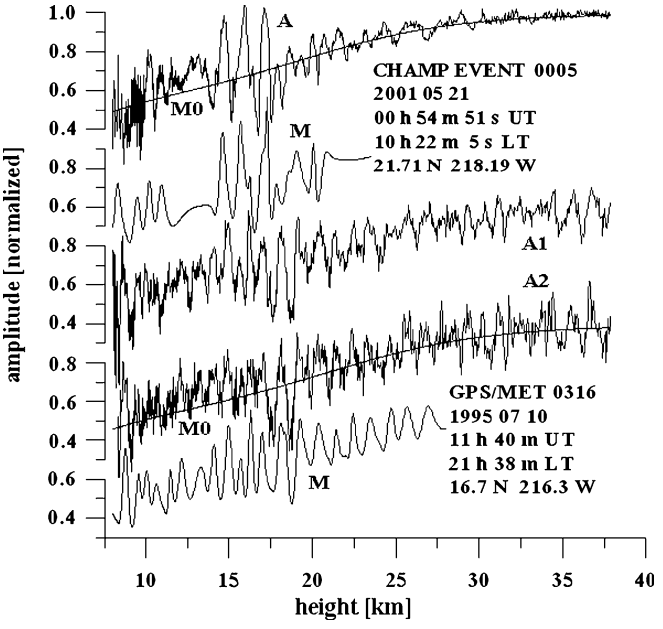

Fig. 2
Wave trains in the GPS/MET and CHAMP RO amplitude data. Legend indicates the time of the RO experiments and the geographical co-ordinates of the RO regions

was a sum of damped complex exponentials $N(h)=\mathrm{Re}[N_j\exp(-\alpha_j h)]$ with real and complex N_j and α_j. The parameters N_j and α_j have been determined such as to give the amplitude variations that coincide with the experimental data.

To obtain the vertical profiles of temperature and its gradient we use expressions by Hocke (1997) and Pavelyev et al. (2002b). The wave train with intense amplitude variations can be noted in the height interval 8–40 km. The waves vertical wavelength is changing in the range 0.8–2 km. The results of the simulation (the curves M0, M in Fig. 2) show a good fit to the experimental data. The result of simulation is in sufficient agreement with the experimental amplitude variations to indicate a low level of possible diffraction effect in the considered events. However, the diffraction effect can be observed in some cases and upgrading of our model will be required. The amplitude changes correspond to variations in the refractivity and temperature vertical gradients. The latter can be restored by the amplitude method described by Kalashnikov et al. (1986); Pavelyev et al. (2002a, 2002b); and Liou et al. (2002).

The vertical gradients of the temperature retrieved from the amplitude data are indicated for CHAMP (the bottom curves A and M) and GPS/MET RO (the upper curves A1, A2 and M) events 0005 and 0316 in Fig. 3. Note that in contrast to the case of the GPS/MET RO experiments, in the CHAMP RO experiments only the amplitude variations at the first GPS frequency F1 has been measured. The curves M in Fig. 3 indicate the simulation results relating to the CHAMP (the second curve from bottom in Fig. 3) and GPS/MET (the second upper curve in Fig. 3) RO events; the curves A1, A2, and A describe the vertical temperature gradient variations restored from the initial amplitude changes shown in Fig. 2. It is evident from Fig. 3 that the wave activity in the atmosphere is a complex function of height. Maximum of the wave activity is observed in the tropopause region in the height interval 12–17 km. Secondary maxima of the wave activity can be seen in the stratosphere in the height interval 22-27 km. Quasi-regular wave structure with vertical wavelength λ_v of 0.8–2 km is clearly seen in both experimental and model data. The observed waves in the altitude distribution of the amplitude and vertical temperature gradient can correspond to the GW activity. If the observed wave structures are caused by the GW activity then the vertical temperature gradients can be related with horizontal wind perturbations associated using the GW polarization and dispersion equations.

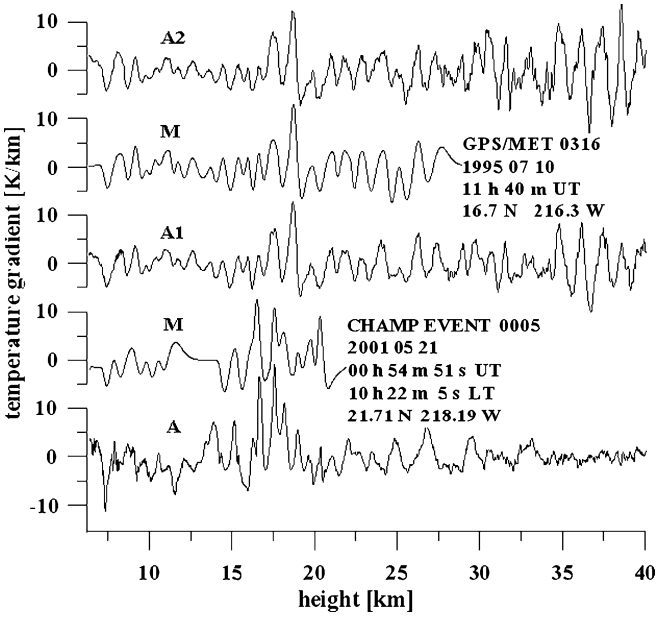

Fig. 3
Temperature gradient variations for the GPS/MET and CHAMP RO events

"Portrait" of the gravity waves

We will use the polarization relationships, which are valid for the medium-frequency case, when the intrinsic frequency of the GW is greater than the inertial frequency f, but is well below the buoyancy frequency ω_b. The GW dispersion relation has the form (Fritts and Alexander 2003; Eckermann et al. 1995)

$$\lambda_v = 2\pi|c - U\cos\varphi|/\omega_b \qquad (16)$$

where λ_v is the vertical wavelength of the GW, U is the background wind speed, c is the ground-based GW horizontal phase speed, and ϕ is the azimuth angle between the background wind and the GW propagation vectors.

En. (16) connects the vertical wavelength λ_v with the intrinsic phase speed of the GW $v_i=(c-U\cos\phi)$, which can be measured by an observer moving with the background wind velocity (Eckermann et al. 1995). A GW polarization relation was published earlier by Lindzen (1981). It connects the complex amplitude of the temperature variation, $t(h)$, with the horizontal wind perturbations $v(h)$, corresponding to the GW influence

$$v = \mathrm{Re}[ig/(T_b\omega_b)t(h)] \qquad (17)$$

where $\omega^2{}_b=g/T_b\Gamma$, $\Gamma=\partial T_b/\partial h+9.8^\circ$/km, g is the gravity acceleration, and T_b is the background temperature. Pfister et al. (1993) applied this relation successfully to the case study of the regular GW associated with tropical cyclone. Eckermann et al. (1995) used it for statistical analysis of the rocketsonde data. Using the RO data, Tsuda et al. (2000) applied relation in Eq. (17) to determine a global distribution of the GW potential energy . One can obtain from Eq. (17) a connection between the vertical gradients $dv(h)/dh$ and $dt(h)/dh$:

$$\begin{aligned} dv(h)/dh &= d\mathrm{Re}[ig/(T_b\omega_b)t(h)]/dh \\ &\approx \mathrm{Re}[ig/(T_b\omega_b)dt(h)/dh] \end{aligned} \qquad (18)$$

Equation (18) is valid assuming that $T_b(h)$ and $\omega_b(h)$ are slowly changing at the vertical scales $\sim\lambda_h$. The functions T_b and ω_b are known from the model of the atmosphere

used for calculating the refraction attenuation and refractivity in the RO region.

To find the function $dv(h)/dh$ from the second Eq. (18) one can implement the radio holographic analysis by applying the Hilbert transform (Rabiner and Gold 1978). We suggest that the amplitude variations are a real part of some analytical function. Under this assumption the temperature vertical gradient and the horizontal wind perturbations are also the real parts of the analytical functions, which are connected with the amplitude variations by inversion formulas and polarization relationship (Liou et al. 2002). The Hilbert transform is a mathematical tool to find the imaginary part of an analytical function using its real part. Practical implementation of the Hilbert transform gives the analytic presentation of the real signal $dt(h)/dh$:

$$dt(h)/dh = Re\{a_t(h)\exp[i\Phi_t(h)]\} \quad (19)$$

where the real functions, $a_t(h)$ and $\Phi_t(h)$, are the amplitude and phase of the vertical gradient of the temperature. Then the function $dv(h)/dh$ can be restored from Eq. (18) using the Hilbert transform applied to the experimental and model data, respectively.

The results of restoration are indicated in Fig. 4. The upper three curves (A1, A2, M) in Fig. 4 correspond to the vertical gradient of the horizontal wind perturbations restored for the GPS/MET RO event 0316, while the bottom two curves (M, A) relate to the CHAMP RO event 0005. The quasi-regular modulation of dv/dh by the wave structures in the atmosphere is clearly seen both in the experimental and model data. It is important that the vertical period of this modulation is practically the same as seen in the amplitude variations in Fig. 3.

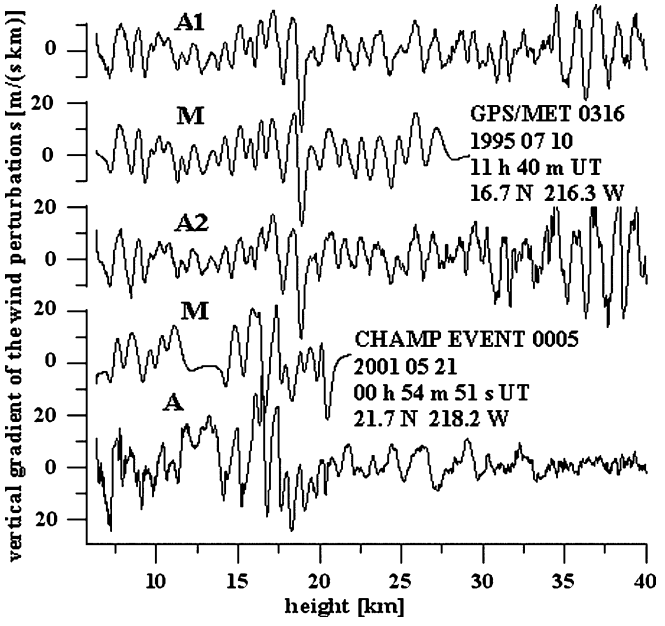

Fig. 4
Vertical gradient of the horizontal wind perturbations retrieved on the variations of the vertical temperature gradient for GPS/MET (*three upper curves*) and CHAMP (*two bottom curves*) RO events

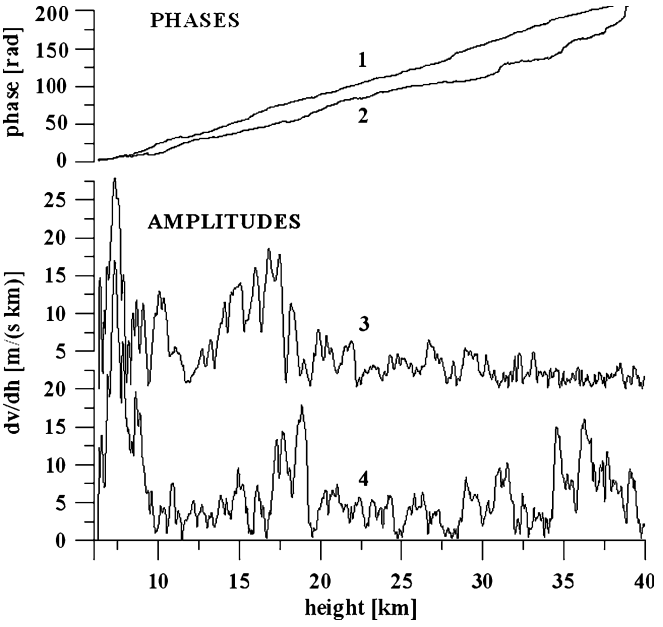

Fig. 5
Comparison of the GW portraits found from the wave trains in the amplitude data for GPS/MET (*curves 1, 4*) and CHAMP (*curves 2, 3*) RO data

After applying the Hilbert transform one can obtain from Eqs. (18) and (19), the amplitude $a(h)$ and phase $\Phi(h)$ associated with the vertical gradient of the horizontal wind perturbations $dv(h)/d\,h = a(h)\cos\Phi(h)$, where $a(h)$ and $\Phi(h)$ are the amplitude and phase of the analytic signal relevant to $dv(h)/dh$. The functions $a(h)$ and $\Phi(h)$ together present a GW "portrait". The height dependence of the GW phases $\Phi(h)$ and amplitudes $a(h)$ are shown in Fig. 5 by curves 1, 2 and 3, 4, respectively, for the GPS/MET and CHAMP RO events 0316 and 0005. The phase curves 1, 2 of the GW portrait have different dependence in relation to the height for the GPS/MET and CHAMP RO events. The phase curve 2 relevant to the CHAMP event indicates increasing spatial frequency of the GW with height. The phase in the GPS/MET event (curve 1 in Fig. 5) changes linearly, in average, as a function of height h, thus corresponding to nearly monochromatic GW. The amplitude, relevant to the GPS/MET event (curve 3 in Fig. 5), demonstrates essential changes in the interval 0.5–16 m s km above 10 km. For this event, one can see from Fig. 5 altitudes with high (17–19, 29–31, 35–38 km) and low (32–34 km) GW activities. For the CHAMP RO event (curve 4 in Fig. 5), the amplitude changes are concentrated mainly below 20 km. It follows from Fig. 5 that the GW radio images contain important information on the height distribution of the GW activity in the RO regions. Another example of the GW activity in the atmosphere is given in Fig. 6 for the GPS MET RO event 0492. The curves 1 and 2 demonstrate the height dependence of the phase and amplitude of the GW. The vertical profile $dv(h)/dh$, curve 2 in Fig. 6, indicates the region of the growing and breaking of the GW at heights 15–18, 20–22, 24–25, and 30–35 km. The position of the GW breaking zone in the height interval 35–37 km is coinciding with the early satellite observations of the mountain waves activity in the

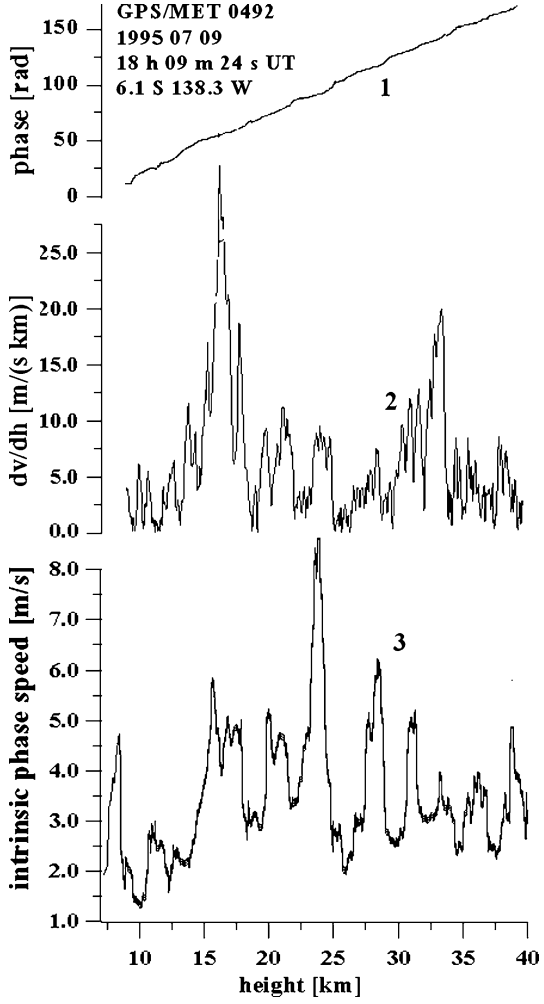

Fig. 6
GW portrait for the GPS/MET RO event 0492 with intense variations in the height interval 30–35 km (*curves 1, 2*). Intrinsic phase speed of the GW as a function of height for the GPS/MET RO event 0492 (*curve 3*)

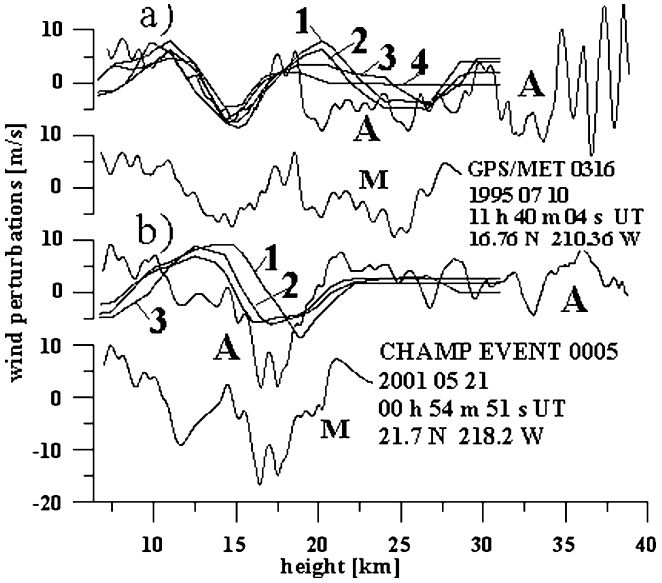

Fig. 7
Comparison of the wind perturbations found from GPS/MET and CHAMP RO events with Earth-based radiosondes data

Andes area provided by Eckermann and Preusse (1999). The phase curve 1 in Fig. 6 reveals the quasi-linear dependence on the height thus indicating quasi-monochromatic character of the observed wave structure. The detailed information on the height distribution of the spatial frequency of the GW can be obtained by differentiating the phase $\Phi(h)$ (curve 1 in Fig. 6). After differentiating one can obtain the spatial frequency f and the vertical wavelength $\lambda_h=1/f$ as functions of height and then estimate the intrinsic phase speed of the GW v_i (curve 3 in Fig. 6) using the relation in Eq. (16). As seen in Fig. 6 (curve 3) the value $v_i(h)$ changes in the range 1.4–8 m/s. These values of the intrinsic phase speed are similar to the intrinsic phase speed observed by rocketsondes (Eckermann et al. 1995) and satellite (Eckermann and Preusse 1999), and may correspond to the quiet conditions in the atmosphere.

Integration of the vertical gradient $dv(h)/dh$ can reveal the horizontal wind perturbations $v(h)$ as a function of height. The function $v(h)$ is depicted in Fig. 7 for the two RO events: GPS/MET 0316 (Fig. 7a) and CHAMP 0005 (Fig. 7b). The curve A in Fig. 7a) has been obtained by integrating the average wind speed gradient $dv/dh=[dv_1(h)/dh+dv_2(h)/dh]/2$ (curves A1, A2 in Fig. 4 restored from the GPS/MET RO amplitude data. The curve A in Fig. 7b) has been obtained by integrating the wind speed gradient dv/dh corresponding to the bottom curve A in Fig. 4 restored from the CHAMP RO amplitude data. The M curves (Fig. 7a, b) describe the results of the simulation. The curves 1–4 in Fig. 7a indicate the radiosondes (RS) data corresponding to two stations in Taiwan: Hualian (1, 4; 24.0°N, 238.4°W) and Taipei (2, 3; 25.0°N, 238.5°W), obtained on July 15, 1995 at 00 h UT (1, 2) and 12 h UT (3, 4), respectively. The curves 1–3 in Fig. 7b) data correspond to the same stations and indicate the RS data obtained on May 30, 2001 at 00 and 12 h UT (1, 2) (Taipei) and 12 h UT (3; Hualian), respectively. The difference between the Taiwan Earth-based stations and the GPS/MET RO region latitudes for the event 0316 is about 8°, the corresponding value for longitudes is about 28°. The difference between the Taiwan and the CHAMP RO region latitudes for the event 0005 is about 3°, the corresponding value for longitude is about 20°. The time difference between the RO events and RS observations has been chosen in accordance with the average background westward wind velocity of about 6–10 m s in the height interval 8–30 km. The RS wind perturbations (curves 1–4 in Fig. 7a) curves 1–3 in Fig. 7b) have been obtained by subtracting the polynomial approximation of the fifth power from the experimental vertical profiles of the horizontal wind speed. As follows from Fig. 7a, the RS data (1–4) are in fairly good agreement with the results found from the amplitude of the RO signal and simulation (curves A, M in Fig. 7a, respectively). Some discrepancy of about ±1–3 m s exists in the height interval 19–30 km. The difference of the CHAMP data (curve A in Fig. 7b from the RS data (curves 1–3 in Fig. 7b) is greater by about

±3–5 m s. Note that the RS data do not reveal high-spatial frequencies observed in the RO results. It appears this is due to smoothing effects of the RS measurements. The RO values of $v(h)$, which corresponds to curves A in Fig. 7, vary from ±1 to ±12 m s at the height interval 10–35 km and indicate some higher magnitudes for the $v(h)$ as compared with the model results (curves M in Fig. 7). The difference illustrates a current state of the inversion accuracy.

Conclusions

The amplitudes of the RO signals at both GPS frequencies are much more sensitive to the wave structures in the troposphere, stratosphere and mesosphere than are the phases. The amplitude wave trains in the RO data can be used for retrieving the phase and amplitude of the wave structures in the atmosphere as functions of height. This property of the amplitude of the satellite signals is important for direct measurements of the regular distribution of the GW activity on a global scale in the height interval 5–40 km. For analysis of the amplitude variations, a new analytical method is introduced. The method uses the polarization and dispersion relations and Hilbert transform to restore the portrait of the GW (the amplitude and phase of the GW as functions of height). The analytic form of the GW presentation is convenient for the analysis of the experimental data and can be implemented for the determination of the GW intrinsic-phase speed and the horizontal wind perturbations associated with the GW influence. For a validation of the new retrieval methods, we compare the wind speed perturbations retrieved from the GPS/MET and CHAMP RO data to the corresponding wind measurements obtained in situ by nearby balloon radiosondes. The radiosonde measurements agree well with the analyzed GPS observations. The discrepancy is about 1–2 m s for the heights below 18 km and 2–4 m s for heights of 20–30 km. The vertical gradients of the horizontal wind speed changed more significantly from ±0.5 up ±16 m s km. Thus, the RO method appears to have considerable promise in measuring the regular characteristics of the GW and the consequent vertical distribution of the horizontal wind perturbations.

Acknowledgments We are grateful to UCAR for access to the GPS/MET data. We are grateful to the National Science Council (NSC) and the National Space Program Office (NSPO) of Taiwan, R.O.C., for financial support under the grants NSC 92-2811-M008-001, 92-NSPO(B)-RS3-FA07-03, and the U.S. Office of Naval Research (ONR) under grant N00014-00-0528. Work has been partly supported by the Russian Fund of Basic Research, Grant No. 03-02-17414.

References

Anthes RA, Rocken C, Kuo Y-H (2000) Applications of COSMIC to meteorology and climate. Terr Atmos Ocean Sci 11:115–156

Dewan EM, Good RE (1986) Saturation and the "universal" spectrum for vertical profiles of horizontal scalar winds in the atmosphere. J Geophys Res 91:2742–2748

Ebel A (1984) Contribution of gravity waves to the momentum heat and turbulent energy budget of the upper mesosphere and lower thermosphere. J Atmos Terr Phys 46:727–737

Eckermann SD, Preusse P (1999) Global measurements of stratospheric mountain waves from space Science 286:1534–1537

Eckermann SD, Hirota I, Hocking WA (1995) Gravity wave and equatorial wave morphology of the stratosphere derived from long-term rocket soundings. Q J R Meteorol Soc 121:149–186

Feng DD, Herman BM (1999) Remotely sensing the Earth's atmosphere using the Global Positioning System (GPS): the GPS/MET data analysis. J Atmos Ocean Technol 16:990–1002

Fritts DC, Alexander MJ (2003) Gravity wave dynamics and effects in the middle atmosphere. Rev Geophys 41:1–64

Hocke K (1997) Inversion of GPS meteorology data. Ann Geophys 15:443–450

Igarashi K, Pavelyev A, Hocke K, Pavelyev D, Kucherjavenkov IA, Matugov S, Zakharov A, Yakovlev O (2000) Radio holographic principle for observing natural processes in the atmosphere and retrieving meteorological parameters from RO data. Earth Planet Space 52:968–875

Igarashi K, Pavelyev A, Hocke K, Pavelyev D, Wickert J (2001) Observation of wave structures in the upper atmosphere by means of radio holographic analysis of the radio occultation data. Adv Space Res 27(6–7):1321–1327

Kalashnikov I, Matugov S, Pavelyev A, Yakovlev O (1986) Analysis of the features of radio occultation method for the Earth's atmosphere study (in Russian). In: Electromagnetic waves in the atmosphere and space. Nauka, Moscow, pp 208–218

Kursinski ER, Hajj GA, Schofield JT, Linfield RP, Hardy KR (1997) Observing Earth's atmosphere with radio occultation measurements using the Global Positioning System. J Geophys Res 102:23–465

Lindzen RS (1981) Turbulence and stress owing to gravity waves and tidal breakdown. J Geophys Res 86:707–714

Liou Y-A, Huang C-Y (2000) Active limb sounding of atmospheric refractivity pressure and temperature profiles from GPS occultation by 3-D vector analysis. Proc. COSMIC Int. Workshop, 27–29 September 2000, Taipei, Taiwan, pp 60–69

Liou Y-A, Pavelyev AG, Huang C-Y, Igarashi K, Hocke K (2002) Simultaneous observation of the vertical gradients of refractivity in the atmosphere and electron density in the lower ionosphere by radio occultation amplitude method. Geophys Res Lett 29(19):1–43

Liou Y-A, Pavelyev AG, Huang C-Y, Igarashi K, Hocke K, Yan SK (2003) Analytic method for observation of the gravity waves using radio occultation data. Geophys Res Lett 30(20):1–5

McFarlane NA (1987) The effect of orographically excited gravity wave drag on the general circulation of the lower stratosphere and troposphere J Atmos Sci 44:1775–1800

Nagpal OP (1979) The sources of atmospheric GWs. Contemp Phys 20:593–609

Nastrom GD, Van Zandt TE Warnock JM (1997) Vertical wavenumber spectra of wind and temperature from high-resolution balloon soundings over Illinois. J Geophys Res 102:6685–6701

Pavelyev A (1998) On the possibility of radio holographic investigation on communication link satellite-to-satellite. J Commun Technol Electron 43(8):126–131

Pavelyev AG, Kucherjavenkov AI (1978) Refraction attenuation in the planetary atmospheres. Radio Eng Electron Phys 23(7):13–19

Pavelyev A, Yeliseyev SD (1989) Study of the atmospheric layer near the ground using bistatic radar. J Commun Technol Electron 9:124–130

Pavelyev A, Volkov AV, Zakharov AI, Krytikh SA, Kucherjavenkov AI (1996) Bistatic radar as a tool for earth investigation using small satellites. Acta Astronaut 39:721–730
Pavelyev A, Igarashi K, Reigber C, Hocke K, Wickert J, Beyerle G, Matyugov S, Kucherjavenkov A, Pavelyev D, Yakovlev O (2002a) First application of radioholographic method to wave observations in the upper atmosphere. Radio Sci 37(3):1–15
Pavelyev AG, Liou YA, Huang CY, Reigber C, Wickert J, Igarashi K, Hocke K (2002b) Radio holographic method for the study of the ionosphere atmosphere and terrestrial surface using GPS occultation signals. GPS Sol 6:101–108
Pfister L, Chan KR, Bui TP, BowenS, Legg M, Gary B, Kelly K, Proffit M, Starr W (1993) Gravity waves generated by a tropical cyclone during the STEP tropical field program: a case study. J Geophys Res 98(D5):8–638
Rabiner L, Gold B (1978) Theory and application of digital signal processing. Prentice-Hall, Englewood Cliffs, New Jersey
Preusse P, Smolarkiewicz JM, Garcia RR (1996) Propagation and breaking at high altitudes of GWs excited by tropospheric forcing. J Atmos Sci 53:2186–2216
Reigber C, Lühr H, Schwintzer P (2002) CHAMP mission status. Adv Space Res 30(2):129–134
Sica R J, Russell AT (1999) Measurements of the effects of GWs in the middle atmosphere using parametric model of density fluctuations, part I: vertical wavenumber and temporal spectra. J Atmos Sci 56:308–1329
Sokolovskiy SV (2000) Inversion of radio occultation amplitude data. Radio Sci 35(16):97–105
Steiner A K, Kirchengast G (2000) Gravity wave spectra from GPS/MET occultation observations. J Atmos Ocean Tech 17:495–503
Steiner AK, Kirchengast G, Landreiter HP (1999) Inversion error analysis and validation of GPS/MET occultation data. Ann Geophys 17:122–138
Tsuda T, Hocke K (2002) Vertical wave number spectrum of temperature fluctuations in the stratosphere using GPS occultation data. J Meteorol Soc Japan 80(4B):1–13
Tsuda T, Nishida M, Rocken C Ware RH (2000) A global morphology of gravity wave activity in the stratosphere revealed by the GPS occultation data (GPS/MET). J Geophys Res 105:7257–7273
Ware R, Exner M, Feng D, Gorbunov M, Hardy K, Herman B, Kuo Y-H, Meehan T, Melnourn W, Rocken, Schreiner W, Sokolovskiy S, Solheim F, Zou X, Anthes R, Businger S Trenberth K (1996) GPS soundings of the atmosphere from low earth orbit: preliminary results. Bull Am Meteorol Soc 77:19–40
Wickert J, Reigber CH, Beyerle G, Konig R, Marquardt CH, Schmidt T, Grunwaldt L, Galas R, Meehan T, Melbourne WG, Hocke K (2001) Atmosphere sounding by GPS radio occultation: first results from CHAMP. Geophys Res Lett 28:3263–3266